Biophysical Chemistry, 47 (1993) 179–191
Elsevier Science Publishers B.V., Amsterdam

BIOCHE 01767

Structure and dynamics of curved DNA fragments in solution: Evidence for slow modes of configurational transitions

Dietmar Porschke [a,*], Erwin R. Schmidt [b], Thomas Hankeln [b], Gerhard Nolte [a] and Jan Antosiewicz [a,**]

[a] *Max Planck Institut für biophysikalische Chemie, D3400 Göttingen (Germany)*
[b] *Institut für Genetik der Universität, D6500 Mainz (Germany)*

(Received 16 December 1992; accepted in revised form 26 February 1993)

Abstract

DNA fragments with unusually low electrophoretic mobility due to intrinsic curvature have been analyzed by comparison of electrooptical data with results of hydrodynamic simulations. Electrooptical data have been collected for three fragments with 161, 196 and 399 base pairs derived from the DNA of *Chironomus thummi thummi* as repetitive elements by Alu I restriction. The dichroism decay time constants reflecting overall rotational diffusion, the bending time constants and the bending amplitudes measured at low salt concentrations (2.4 mM Na^+ and 100 μM Mg^{2+}) are rather close to those observed for standard DNA fragments. At high salt concentration (0.1 M Na^+ and 10 mM Mg^{2+}) the temperature dependence of the overall rotational time constants indicates a slightly increased degree of curvature at low temperature (2°C). The experimental data are complemented by hydrodynamic simulations based on predictions of DNA trajectories given by Bolshoy et al. [*Proc. Natl. Acad. Sci. USA* 88 (1991) 2312]. These trajectories are converted into bead models, which are then subjected to thermal fluctuations using a Monte Carlo procedure. For standard values of the persistence length and the torsional flexibility, thermal fluctuations induce considerable variations of the equilibrium curvature. As a first attempt to find conditions where the predicted trajectories are consistent with our hydrodynamic data, we tested a model with a high internal mobility, which has been commonly applied for standard DNA fragments. However, the overall rotational time constants predicted for this case are clearly smaller than the observed ones, even at high values of the persistence length. Then, we simulated time constants in the limit of low internal mobility by calculation of electrooptical transients for large numbers of individual configurations. The average of these transients could be fitted by two exponentials at high accuracy, although the simulations led to broad distributions of configurations. In this respect the simulated curves are very similar to the experimental ones. For standard values of the persistence length and of the torsional flexibility, the large time constants τ_2, reflecting overall rotational diffusion, are still smaller than the experimental ones. τ_2-values simulated as a function of the persistence length p show a maximum, which appears at $p \approx 1000$ Å for the Alu-fragments. The τ_2-values simulated at these maxima are consistent with the experimental ones within the limits of accuracy. Thus, provided that the curvature has been estimated correctly by the model based on gel mobilities and on circularization experiments curved DNA fragments show

* To whom correspondence should be addressed.
** On leave from Department of Biophysics, Warsaw University, 02-089 Warsaw, Poland.

a relatively low rate of the internal dynamics and also appear to be less flexible than standard DNA's with respect to the dynamic persistence. The difference in the dynamic persistence is negligible, however, if the apparent persistence length of standard DNA has a major contribution from intrinsic curvature, corresponding to an average static persistence length of about 800 Å. In summary, our results indicate that the "deviations from linearity" of our curved fragments are not much different from those of standard DNA's; however, our results are consistent with the view that curved DNA fragments are "curved" preferentially in one direction with relatively slow modes of configurational transitions and with a relatively high rigidity, whereas standard DNA is subject to bending by thermal motion in all directions with (almost) equal probability.

Keywords: Electrodichroism; Rotational diffusion; Bead model simulations; Flexibility, bending and torsional

1. Introduction

The assignment of "curvature" to special DNA fragments has been mainly based on unusual mobilities in gel electrophoresis [1,2]. Various experimental data have been presented as supporting evidence for DNA curvature, including electrooptical data with particularly high rotational diffusion coefficients for curved DNA samples [3–5]. However, in one of the electrooptical investigations it was found that curved DNA fragments could hardly be distinguished from standard DNA fragments according to their rotational diffusion [6]. This is a challenge in view of the high degree of curvature suggested for these special fragments and the very high sensitivity of electrooptical decay curves to variations in the effective hydrodynamic length; for example, the length increase caused by insertion of a single intercalator like ethidium into a double helix with 100 bp can be easily detected by electrooptical measurements [7]. As a first attempt to explain the unexpected observation, it has been proposed that stretching of curved DNA by electric field pulses may be "inelastic", in the sense that stretched fragments return to their equilibrium state of curvature with a time constant larger than that for overall rotational diffusion [6]. However, in this case curved DNA fragments would have to be stretched considerably already at rather low electric field strengths and, thus, the bending stiffness of curved DNA would have to be relatively low. Furthermore, a recent quantitative investigation of field induced stretching showed that the stretching effect remains small at low electric field strengths [8]. Finally, the dichroism decay time constants have been measured down to electric field strengths of a few kV/cm and also have been extrapolated to zero field strength; thus, the influence of field induced changes of the structure, if existent at all, on the resulting time constants should be negligible. Some laboratories have reported reduced electrooptical decay time constants for curved DNA fragments, but not all of these reports can be taken as conclusive [2].

Because DNA curvature has been confirmed by enzymatic circularization experiments [9,10] and also appears to be visible by electron microscopy [11], the existence of curved DNA can hardly be questioned. However, the physical mode and the degree of curvature remains to be established. In this context, electrooptical methods should be very useful for the characterization of curved DNA structure and dynamics in solution because of their particularly high sensitivity.

In our present investigation we have extended the set of electrooptical data by measurements on some DNA fragments with unusually low gel mobility using the "standard" equipment applied at low salt concentrations. In addition, we have used a new electrooptical technique [12], which has been developed for measurements at physiological salt concentrations. Finally, we present model calculations on the hydrodynamics of curved DNA fragments. These calculations are based on the estimation of all 16 DNA wedge angles by Bolshoy et al. [13]. The DNA structures predicted by Bolshoy et al. (cf. also [14]) have been converted to bead models [15,16], bending and torsional flexibility [17,18] have been introduced using Monte Carlo procedures and electrooptical tran-

sients have been calculated [19]. By comparison of experiments and model calculations we derive information on the structure and dynamics of curved DNA in solution.

2. Materials and methods

The DNA fragments were prepared from a pUC 18/19 plasmid containing an insert isolated from the DNA of *Chironomus thummi thummi* as a repetitive element by Alu I restriction [20]. This plasmid was cut by the restriction nucleases Eco RI and Hind III. From the digest, the fragment Alu-T with 399 bp (+4 Hind III/4 Eco RI single stranded residues at the ends) was isolated by high performance liquid chromatography (HPLC) on Nucleogen (Macherey-Nagel, Düren, Germany) according to the procedure of Colpan and Riesner [21]. Part of this fragment was digested further with Ssp I and Bam HI. Final separation by HPLC provided the fragments Alu-1 with 161 bp (+4 single stranded "Bam HI" residues) and Alu-2 with 196 bp (+4 single stranded "Eco RI" residues), without contaminations according to gel electrophoresis.

The fragments were dialysed extensively: first against 1 *M* NaCl, 1 m*M* Na-cacodylate pH 7.0, 0.2 m*M* EDTA; part of the samples were then dialysed against 1 m*M* NaCl, 1 m*M* Na-cacodylate pH 7.0, 200 μM EDTA (buffer E) and another part against 1 m*M* NaCl, 1 m*M* Na-cacodylate pH 7.0, 100 μM $MgCl_2$ (buffer M). For the measurements in the high salt buffers A (100 m*M* NaCl, 1 m*M* Na-cacodylate pH 7.0, 200 μM EDTA) and C (100 m*M* NaCl, 10 m*M* Na-cacodylate pH 7.0, 10 m*M* $MgCl_2$) the components were added to the samples in buffers E and M, respectively.

The electric dichroism at low salt concentrations was measured using a pulse generator [22] and an optical detection system [23] described previously. The electric field pulses in the range of 2 to 70 kV/cm were applied to the samples in a cell with 10 mm optical path length and a distance between the Pt-electrodes of 6 mm. UV-radiation damage was avoided by the use of an automatic shutter which was opened only for short periods of time synchronized to the field pulses. The transmission at 248 nm and the electric field strength as a function of time were recorded by a Tektronix 7612D digitizer.

The electrooptical data at high salt concentration were obtained using a recently developed instrument, described in detail elsewhere [12]. The pulse generation is based on the cable discharge technique with pulses up to 45 kV for 200 ns and rise/decay times of a few ns. The limit time resolution of the optical detection unit also is a few ns. The cell has 5 mm optical pathlength and a distance of 5 mm between the Pt-electrodes. The instrument is driven by a personal computer with automatic sampling via a transient recorder (Tektronix 7612D and 7912AD), online control of the sample temperature and minimal exposure of the sample to UV-light by a computer driven shutter.

The computer programs used for simulation of electrooptical decay curves were as described previously (cf. [16]). All decay curves were simulated for a temperature of 20°C using a viscosity of 1.002×10^{-3} kg m^{-1} s^{-1} corresponding to dilute aqueous solutions. The diagonal components of the local extinction coefficient tensor were 9100, 9100 and 1300 corresponding to an extinction coefficient of 6500 M^{-1} cm^{-1} and a limit value of the linear reduced dichroism of -1.2. The polarizabilities were calculated assuming a quadratic increase with the chain length for straight fragments according to $p_N = N^2 \times 7.496 \times 10^{-37}$ [Cm^2 V^{-1}] (from experimental data obtained for standard DNA fragments in buffer M; Porschke, to be published). The polarizability tensor of curved fragments was calculated by simple addition of local contributions according to the procedure described by Antosiewicz and Porschke [24]. Amplitudes of dichroism decay curves were calculated under the approximation of the Kerr formalism (cf. [19]) using an electric field strength of 10 kV/cm.

The DNA chains were represented by beads with a radius of 12.5 Å; for the fragment Alu-T base pairs were substituted by beads at an interval of $n = 4$ base pairs (cf. below); for Alu-1 and Alu-2 we used $n = 3$. Simulations are also given for the fragment "p*K* 5" (108 bp), which is pre-

dicted to be strongly curved but showed dichroism decay time constants close to those of standard DNA's in a previous investigation [6]; in this case we used $n = 2$. Because of the bead radius $r = 12.5$ Å, beads centered at terminal base pairs add a hydrodynamic equivalent of three base pairs; this effect has been corrected by "deleting" three base pairs at blunt ends; four single stranded residues at both ends were counted as an hydrodynamic equivalent of five base pairs (cf. [25]); four single stranded residues at one end were counted as an equivalent of two base pairs. The experimental dichroism decay curves were evaluated by an efficient deconvolution routine [26], whereas the simulated decay curves were fitted by the program "DISCRETE" of Provencher [27].

3. Results

3.1. Electrooptical experiments

In general, the electrooptical data obtained for curved DNA fragments are very similar to those observed for standard DNA fragments. Thus, we do not have to describe the electrooptical experiments in detail, but simply present the results. Whenever the observed time constants showed a dependence on the electric field strength, the values were extrapolated to zero field strength.

As described in previous communications [28–30] dichroism decay curves for fragments with chain lengths $N \gtrsim 100$ bp require more than single exponentials for satisfactory fits. For the fragments Alu-1 and Alu-2 two exponentials were sufficient. The slow component represents overall rotational diffusion, whereas the fast one is assigned to bending of the DNA double helix. For Alu-T three exponentials were required, where again the slowest one represents overall rotational diffusion and the faster ones segmental motion and/or bending. The slow time constants are compiled in Table 1 and the data on bending for Alu-1 and Alu-2 in Table 2.

Table 2

Bending time constants (ns) from dichroism decay. Bending amplitudes at 70 kV/cm are given in round brackets. Estimated accuracy: data for buffer E ± 10%; data for buffers A and C ± 20%

Temperature (°C)	Alu-1			Alu-2	
	E	A	C	E	C
2	220 (32%)	370	310	290 (34%)	490
10		370	280		280
20	130 (30%)	320	210	200 (36%)	250
30	110 (30%)			170 (37%)	

A first comparison shows that the data obtained for the curved fragments are rather close to corresponding ones measured for standard DNA fragments. Some indication for a special property of curved fragments comes from the temperature dependence of the overall rotational time constants. While these constants measured in the low salt buffer E scale with the standard viscosity/temperature conversion factor, some deviation is found in the data collected in the high salt buffer: the overall rotation at 2°C is somewhat faster than expected from the 20°C data after viscosity/temperature conversion. This suggests a higher degree of curvature induced at

Table 1

Overall rotational diffusion time constants [μs] from dichroism decay. Estimated accuracy: data for buffer E ± 2%; data for buffers A and C ± 6%. The numbers in parentheses represent the ratios of the respective time constants to those measured at 20°C; the numbers expected according to the temperature/viscosity conversion factor are 1.78, 1.35 and 0.77 for 2, 10 and 30°C, respectively

Temperature (°C)	Alu-1			Alu-2		Alu-T
	E	A	C	E	C	E
2	3.79 (1.75)	3.14 (1.34)	3.25 (1.50)	5.91 (1.81)	5.18 (1.63)	27.4 (1.62)
10		2.93 (1.25)	2.91 (1.34)		3.60 (1.13)	24.0 (1.42)
20	2.16 (1.00)	2.34 (1.00)	2.17 (1.00)	3.27 (1.00)	3.18 (1.00)	16.9 (1.00)
30	1.68 (0.78)			2.64 (0.81)		

low temperatures, in agreement with current views on the temperature dependence of DNA curvature [2].

3.2. Bead model simulations

3.2.1. Configurations of curved DNA

Investigations of the inherent curvature of DNA double helices during recent years have led to a detailed models for the trajectories of curved DNA fragments [13,14]. We have used the model of Bolshoy et al. [13] for the simulation of electrooptical transients for our fragments and have tested, whether the model and our experimental data are consistent with each other. For a comparison of the structures proposed for curved DNA fragments with the results of our electrooptical experiments we have used the following procedure.

We started from the experimental estimation of all 16 DNA wedge angles by Bolshoy et al. [13] and also used their program, generously given to us by A. Bolshoy and E. Trifonov, for the calculation of DNA coordinates from these wedge angles. This program generates the coordinates of phosphate residues and of the centers of base pairs, as shown in the example given in Fig. 1a. For the calculation of hydrodynamic parameters, the base pairs (or a given fraction of base pairs) were converted into beads: the centers of the

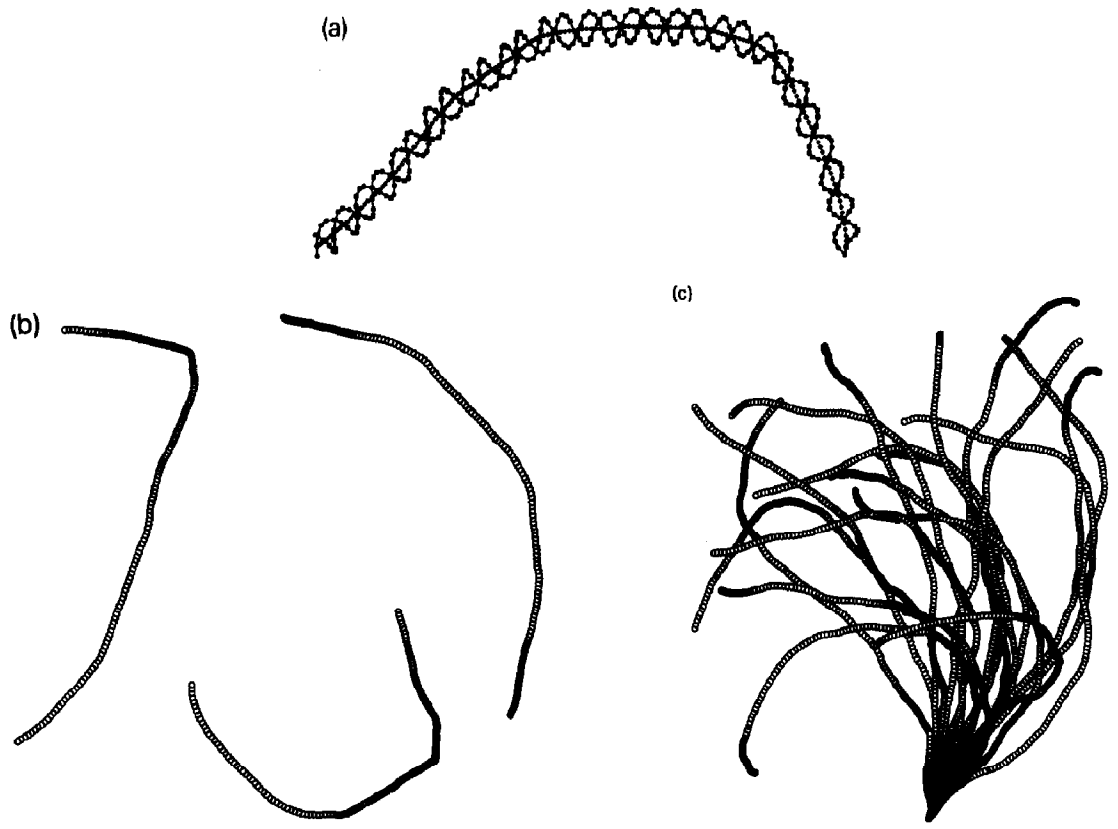

Fig. 1. (a) View of the DNA trajectory predicted by the procedure of Bolshoy et al. for the fragment Alu-1. (b) Each of the nucleotide residues of the model in (a) is replaced by a bead of 12.5 Å diameter; the resulting model is shown in 3 different orthogonal views. (c) A random selection of 20 configurations generated by a Monte Carlo procedure using a persistence length of 450 Å and a torsional elastic constant of 2×10^{-19} erg cm at 20°C. The first two beads of each configuration are superimposed.

beads were placed to the centers of base pairs predicted by the program of Bolshoy et al.; the bead radius was 12.5 Å. The resulting bead model has been used to calculate hydrodynamic parameters according to the procedures discussed by Garcia de la Torre and Bloomfield [15] using a modification developed by Antosiewicz and Porschke [16].

The bead models generated by the procedure described above are stiff, whereas DNA double helices are flexible: both bending and torsional flexibility have to be considered, at least for chain lengths ≥ 100 base pairs. Bending and/or torsion may occur at any site of the double helix and, thus, the number of possible configurations is infinitely high. We generate representative ensembles of these configurations by the following procedure:

The trajectory predicted by the program of Bolshoy et al. is assumed to represent equilibrium bending and torsion angles. Deviations from the equilibrium bending angles are described by a perturbation angle α_i, which is taken from the distribution

$$F(\alpha_i) = F_c\, e^{-\alpha_i^2/2\sigma_\alpha^2}$$

with

$$\sigma_\alpha = \sqrt{n\,h/p}$$

where n is the number of steps between subsequent beads in units of base pairs, h the helix rise per base pair, p the persistence length and F_c a normalization factor. The direction of the bending perturbation is assumed to be isotropic and is chosen with equal probability between 0 and 2π. The torsional perturbation angle ψ is taken from a normal distribution around zero with the standard deviation

$$\sigma_\psi = \sqrt{kT\,n\,h/C}$$

where kT is the thermal energy and C the torsional elastic constant.

Perturbation angles have been calculated for each bead to bead connection leading to an individual "perturbed" configuration. It should be useful to look at the variations of the configuration imposed on DNA double helices by Brownian motion. Based on the coordinates of the model predicted by the data of Bolshoy et al. (cf. Fig. 1a), we generate the bead model, which is presented in 3 different views in Fig. 1b. Then, we apply the Monte Carlo algorithm for the generation of thermal fluctuations. A random selection of 20 different configurations (cf. Fig. 1c), calculated with standard values of the persistence length (450 Å) and of the torsional elastic constant (2.0×10^{-19} erg cm) clearly demonstrates the large amplitude of fluctuations imposed on the DNA by thermal motion. Due to the large variation of the configurations, experimental data have to be simulated for large ensembles of these configurations, in order to arrive at some representative average. The averages given below have been calculated for at least 10^4 randomly generated configurations.

3.2.2. High rate of internal mobility

It is not sufficient to include large numbers of different configurations, but we have to consider also the rate of conversion between different configurations. Usually it is assumed that the configurations are converted into each other at very high rates. In this case representative time constants can be calculated from averages of the overall rotational diffusion coefficients for individual configurations (cf. [17]). We have used this procedure with various values of the persistence length and of the torsional elastic constant. In all cases, the simulated time constants are much lower than the experimental ones (values are included in Figs. 3, 4 and 5). We have checked by controls with straight DNA models that the results of our simulation procedure are consistent with results published previously (e.g. [17]).

3.2.3. Time constant of internal conversion larger than overall rotational time constant

Because we cannot explain our experimental data by the model based on high internal mobility, we test the other extreme and do simulations for the case of low internal mobility. This case may be simulated by the calculation of electrooptical transients for individual configurations. The averages of transients calculated for large num-

bers of configurations are then evaluated in complete analogy to experimental data by standard exponential fitting routines. This procedure is correct in the limit, where the rate of internal motions is low relative to the rate of overall rotational diffusion.

The input data required for the simulation of electrooptical transients are the tensors of diffusion coefficients, of extinction coefficients, of the polarizability and/or a vector of the permanent dipole moment [19]. Contributions from a permanent dipole moment are usually neglected in electrooptical calculations for DNA double helices and, thus, we present calculations without consideration of permanent dipole contributions first. The tensor of diffusion coefficients is obtained from the bead model simulation, the tensor of extinction coefficients is calculated on the basis

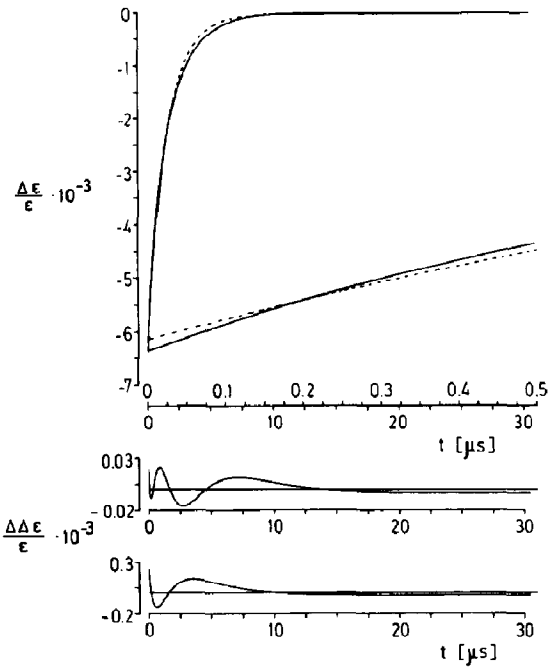

Fig. 2. Electrooptical decay curve simulated for the fragment Alu-1 using a persistence length 800 Å, a torsional elastic constant of 1×10^{-19} erg cm and an effective phosphate charge zero (average of 3×10^4 chains). The simulated data and the fit by two exponentials ($\tau_2 = 1.97$ μs, 77.8% of the total amplitude; $\tau_1 = 0.494$ μs) cannot be distinguished; the dashed line represents a fit by a single exponential. The upper and the lower $\Delta\Delta\varepsilon/\varepsilon$-traces show the residuals for the two and the one-exponential fit, respectively.

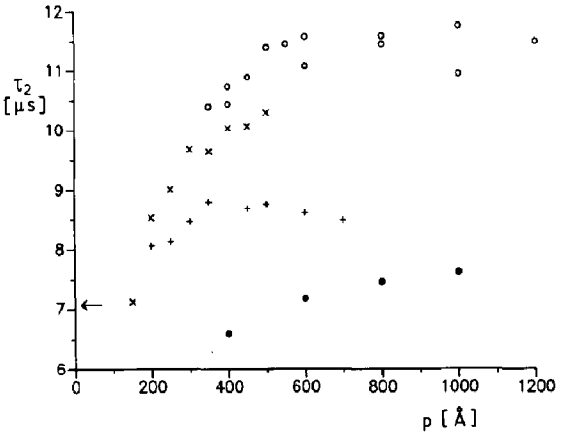

Fig. 3. Slow time constants τ_2 from electrooptical decay curves simulated for the fragment Alu-T at different persistence lengths p; torsional elastic constants $C = 2\times10^{-19}$ (+ and ×) and 1×10^{-19} (○) in erg cm; effective phosphate charges $q = 0.15e$ (+) and 0.0 (× and ○); 20°C. Some time constants calculated from averaged coefficients for overall diffusion for the case $C = 1\times10^{-19}$ are given for comparison (●). The τ_2-value calculated for the rigid limit case and zero phosphate charge is indicated by the arrow.

of the model structure resulting from the program of Bolshoy et al.; finally, the polarizability tensor is calculated by simple addition of local contributions based on experimental data obtained for standard DNA fragments [24].

The dichroism decay curves simulated from these input parameters (and also from the input parameters discussed below) under the assumption of a low internal mobility require two exponentials for a satisfactory fit (cf. Fig. 2), for all the helices included in our present investigation. In this respect the simulated decay curves are very similar to the experimental ones. Although there is a continuous distribution of chain configurations in solution and an almost continuous distribution in the simulation, the observed electrooptical decay curves can be represented by two exponentials at a high accuracy. For molecules with high internal mobility, each of the configurations may be quickly converted into other ones, resulting in a fast coupling mode between the different configurations, which may contribute to the observation of a lower number of exponentials than may be expected otherwise. However, fast coupling is not included in this simulation

and, thus, another explanation must be given for the observation of a relatively low number of exponentials. Apparently, the hydrodynamic parameters of the different configurations do not vary as much as may be expected according to Fig. 1c and a dominant part of the exponentials "falls" in a relatively narrow range. This may be partly due to the fact that compact configurations do not contribute to the electrooptical signal as much as extended ones, because compact forms have relatively low optical and electrical anisotropies. Furthermore, it is notoriously difficult to separate a spectrum of superimposed exponentials. The separation of only two exponentials may already be a difficult problem, especially for experimental data with some noise. Although the simulated dichroism decay curves do not have any noise, it is impossible at the given computational accuracy to identify the individual exponential components within the superposition.

Among the two time constants obtained from the simulated decay curves, the larger one, τ_2, indicates the average global structure of the DNA double helices, which is determined by its equilibrium structure and by the bending and torsional flexibility. We started our simulations with the

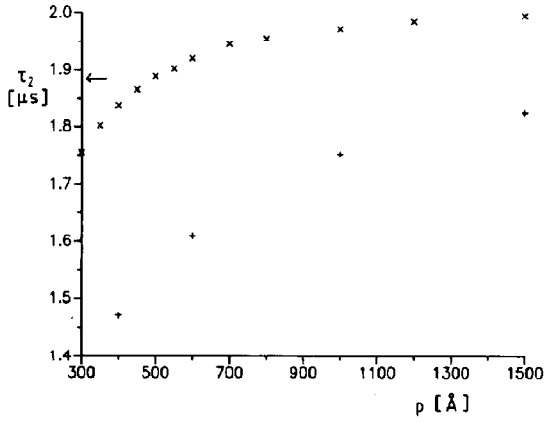

Fig. 4. Slow time constants τ_2 from electrooptical decay curves simulated for the fragment Alu-1 at different persistence lengths p (×). Torsional elastic constant $C = 1 \times 10^{-19}$ erg cm; effective phosphate charge zero. Some time constants calculated from averaged coefficients for overall diffusion are given for comparison (+). The τ_2-value calculated for the rigid limit case is indicated by the arrow.

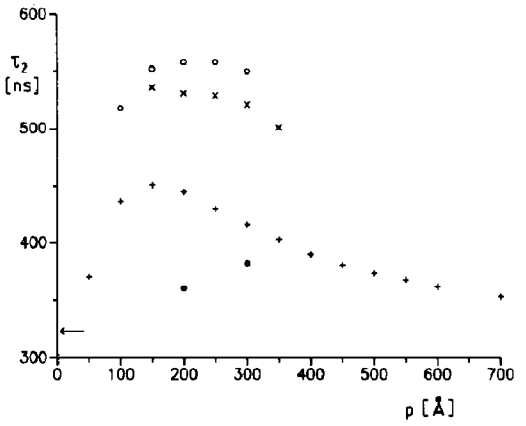

Fig. 5. Slow time constants τ_2 from electrooptical decay curves simulated for the fragment pK 5 at different persistence lengths p; torsional elastic constants $C = 2 \times 10^{-19}$ (+), 4×10^{-19} (×) and 1×10^{-19} (○) in erg cm; effective phosphate charges $0.15e$ (+) and 0.0 (× and ○); 20°C. Some time constants calculated from averaged coefficients for overall diffusion for the case $C = 1 \times 10^{-19}$ are given for comparison (●). The τ_2-value calculated for the rigid limit case and zero phosphate charge is indicated by the arrow.

persistence length and the torsional flexibility found for standard DNA fragments. The time constant resulting from this calculation is larger than the one calculated in the limit of high internal mobility, but still lower than the experimental value. Because the average global structure is strongly affected by the value of the persistence length p, we have studied the influence of the p-value on the magnitude of τ_2. As shown in Fig. 3 for the example of the fragment Alu-T, an increase of p first leads to an increase of τ_2, until a maximal τ_2-value is approached in the range $p = 1000$ to 1200 Å followed by a decrease of τ_2 at $p > 1200$ Å. A corresponding dependence has also been found for the other curved DNA fragments. However, the maximum of the time constant appears at somewhat different p-values for individual fragments, depending on their length and their degree of curvature (cf. Fig. 4 and 5). The τ_2-values found at these maxima are reasonably close to the corresponding experimental time constants.

We have also tested the influence of the torsional flexibility on the averaged overall rotation

time constant τ_2. As may be expected, changes of the torsional elastic constant C do not induce as large variations of τ_2 as found for changes of the persistence length (cf. Fig. 3 and 5).

3.2.4. Effects of "permanent" moments of charged asymmetric configurations

The arrangement of phosphate charges is essentially symmetric for straight double helical DNA and any permanent electric moment of these helices is negligible. However, for curved DNA fragments the distribution of charges is not symmetric anymore and, thus, is associated with large "permanent" dipole moments. The magnitude of these dipoles can be huge, because of the large number of phosphates and because of the large distances between the charges. Calculations for a DNA fragment with 179 bp bent into circular arcs showed that the corresponding dipole moment can be as high as ~3000 D [24]. For these calculations we have used effective phosphate charges, which are reduced in order to account for ion condensation. The degree of ion condensation is predicted by polyelectrolyte theory [31,32] for the case of infinitely long line charges, but is not known with sufficient accuracy for double helices of limited chain length and/or of a given degree of curvature. In our present calculations we have used effective charges associated with the phosphate residues $q \approx 0.15e$, where e is the elementary charge. The dipole moments of molecules with a net charge have to be calculated with respect to the "center of diffusion". We obtain the coordinates of this center from the bead model simulations (cf. Garcia de la Torre and Bloomfield [15]). The direction of the dipole is radial for circular arcs and, thus, results in a special contribution to the alignment tensor.

When the special "permanent" dipole moment is included in our simulations, its contribution leads to a clear reduction of the dichroism decay time constants, as shown in Figs. 3 and 5 for the examples of the fragments Alu-T and pK 5, respectively. The reason for this reduction is indicated by calculations for curved DNA fragments [24]: the permanent electric moment may induce a contribution with a positive linear dichroism, which may lead to an apparent acceleration of dichroism transients or even to the appearance of a maximum in the dichroism transient [33]. Effects corresponding to these predictions have been observed in dichroism experiments, but it has not been possible yet to establish all conditions for the appearance of these special effects quantitatively. One of the difficulties results from the fact that the special effects have been observed only after pulses of sufficient length, which suggests a contribution from some field induced reaction, for example dissociation of ions and/or changes of the curvature. The special effects are suppressed at low salt concentration, which is apparently due to a higher contribution from polarization terms than from permanent moments under these conditions. In analogy, the appearance of the special effects in the simulations may be suppressed by selection of high polarizabilities. The magnitude of the special effects depends, of course, on the magnitude of the phosphate charges and would also be modified by a variation of the residual charge along the DNA chain.

In summary, contributions from permanent moments reduce the time constants simulated for our curved DNA fragments below the experimental ones. The comparison of experimental and simulated data suggests that the contribution from permanent moments is negligible in the case of our curved DNA fragments. A potential reason for the apparent absence of the special dipole effects may be a reduced residual phosphate charge in our fragments and/or a non-homogeneous distribution of these charges along the chain. Obviously, the special phenomena resulting from permanent moments associated with curved DNA fragments require further investigations. A complete quantitative description may be approached by Brownian dynamics simulations with inclusion of the dynamics of both the polymer chain and the ion association.

3.2.5. Fast relaxation processes

The experimental decay curves exhibit relatively large amplitudes for the fast relaxation process(es), when these curves are measured at high electric field strengths $E \geq 10$ kV/cm. It has

been shown that the dominant part of the fast relaxation amplitudes is due to field induced stretching during high electric field pulses, which leads to the reverse process of bending after pulse termination [28–30]. At low electric field strengths $E \leq 5$ kV/cm, the amplitudes associated with fast processes found in the dichroism decay curves are much smaller and are compatible, within experimental accuracy, with the fast amplitudes observed in our present simulations.

4. Discussion

Curved DNA double helices appear to be essential for processing of the genetic information. Thus, the structure of curved DNA segments and their dynamics is of particular interest. We have used electrooptical methods for an analysis of curved DNA, partly because previous experimental results obtained in this laboratory [6] appeared to be in contradiction with current views on the structure of curved DNA [1,2]. The electrooptical measurements described above confirm the unexpected results obtained previously. Now, these unexpected observations cannot be explained anymore by accidental selection of DNA fragments, which may not be representative for some reason. Our present results obtained for an independent set of DNA fragments show that the problem is a more general one and add further evidence that the overall rotational diffusion coefficient of curved DNA fragments is not much different from that of standard DNA of corresponding length.

In our present investigation we have also extended our measurements to high salt concentrations. As may be expected for polyelectrolytes, there is some decrease of the rotational diffusion coefficients, when the salt concentration is increased from a few m M to 100 m M. As shown in a recent investigation of standard DNA fragments [30], the average persistence length is a linear function of the reciprocal square root of the salt concentration. This experimental result is in agreement with numerical calculations on the electrostatic contribution to the bending flexibility [34,35]. The salt dependence observed for curved DNA fragments is similar to that found for standard DNA.

Some indication for a special structure formed at low temperatures and high salt concentrations comes from the temperature dependence of the dichroism decay time constants, which are not consistent with the simple viscosity/temperature conversion factor. These results suggest that the average degree of curvature of our fragments is increased at low temperature [2].

Since detailed models for curved DNA's and reliable procedures for hydrodynamic simulation are available, we have been able to check, whether these models are consistent with our electrooptical results. The experimental results were obtained for fragments with a rather high number of base pairs and, thus, both bending and torsional flexibility had to be included in our simulations. As shown in Fig. 1c, standard values of the flexibility lead to very large variations of the DNA configuration, which appear to be in contrast to the standard schemes shown in the literature. In general, DNA double helices are represented as single, unique structures in the form found in the crystals without any indication for potential variations due to thermal motions. This type of presentation has contributed to the impression that double helices are rather rigid structures. In our simulations, the dynamics of DNA double helices has been described by a Monte Carlo procedure for the generation of individual configurations. These configurations have been used for the simulation of experimental data in the limit cases of high and low internal conversion rates.

The results of these simulations show that our experimental data can only be described in terms of the current view on curved DNA structures, if its flexibility is lower than that accepted for standard DNA double helices. Another potential explanation would be an increased helix rise per base pair for sequences contributing to curvature, which appears to be ruled out, however, by the results of both X-ray fiber diffraction and by high resolution crystal analysis: the main elements contributing to curvature, phased stacks of A–T pairs, exhibit a helix rise per base pair of about

3.2 Å, which is clearly below the average value [36–38]. When we use a high value of the persistence length around 1000 Å and a low rate of internal conversion, the agreement between experimental and simulated data is satisfactory for those fragments, where the experimental time constants are most accurate: for the fragment Alu-1 the experimental and the simulated time constants are 2.2 and 2.0 μs; for Alu-2 we found 3.2 and 3.0 μs (20°C). For the long fragment Alu-T the agreement between the experimental (16.9 μs) and the simulated (11.5 μs) time constants is less satisfactory. Finally, a large disagreement (experimental 1.1 μs, simulated 0.56 μs) remains for the fragment pK 5 for yet unknown reasons. Part of the disagreement may be due to the fact that the dichroism decay of this fragment has been studied only in a low salt buffer containing EDTA; it should be reinvestigated in a buffer containing Mg^{2+}-ions and/or a high salt buffer.

The persistence length found for our curved DNA fragments appears to be in contradiction with values derived for standard DNA by various experimental techniques. However, the data are not directly comparable, because the p-values observed for standard DNA's have been determined under the assumption that the equilibrium configuration of the double helices is straight. It must be expected that some contribution to the standard value of the DNA persistence length results from an intrinsic curvature. The apparent persistence length p_{app} is given by

$$1/p_{app} = 1/p_s + 1/p_d$$

where p_s and p_d are the static and the dynamic persistence lengths, respectively [39–41]. According to definition the static persistence length is attributed to effects resulting from intrinsic curvature, whereas the dynamic persistence length describes the influence of thermal fluctuations. We may use the experimental value $p_{app} = 450$ Å obtained for standard DNA's together with the value derived from our present simulations $p_d \approx 1000$ Å and then arrive at an average static persistence length for standard DNA's $p_s \approx 820$ Å. This p_s-value appears to be reasonable for standard DNA sequences and, thus, the dynamic persistence length required to fit our present experimental data is probably not unusual at all.

It is important to note that the values of the persistence length, including the so-called dynamic persistence length, imply virtually nothing on the relaxation time constant of the transitions between different configurations. As for any intramolecular transition, the transitions between different configurations may proceed anywhere in the time range from ns to s or even to hours or years, depending on the magnitude of the activation barriers. The influence of the equilibrium position on the time constants is negligible in most cases. Usually the rate of conversion between different configurations is assumed to be fast. The existence of fast internal conversions has been demonstrated [8,28,29,42], but the rate of these conversions are expected to be dependent on the sequence, the ionic conditions and certainly on the temperature. Thus, internal conversion may be fast in certain cases and slow in other cases. Moreover, we have to expect that there can be fast and slow modes of internal conversion in the same chain. For example, the stretching of chains under electric field pulses and the reverse process of bending after pulse termination are probably mainly "elastic" and their rate appears to be mainly determined by hydrodynamics. Thus, the close correspondence of bending time constants observed for standard and for curved DNA fragments does not necessarily imply that their dynamics is equivalent in all detail. It is very likely that real activation barriers have to be overcome for certain types of internal transitions. A simple analogy exists in the case of proteins, where *cis–trans* transitions of proline residues are particularly slow and most other internal elementary transitions are orders of magnitude faster. Corresponding barriers are likely to exist also for polynucleotide chains and remain to be identified.

The results of our investigation are different from those obtained previously in several respects. First of all, the dichroism decay time constants obtained for curved DNA fragments obtained in this laboratory are very similar to those of standard fragments, whereas the dichroism decay time constants found in other laborato-

ries [3–5] are somewhat smaller than those of standard fragments. It is not clear, where the difference in the experimental results may come from, but also in the cases reported from other laboratories the difference between the time constants for standard and curved fragments remains smaller than should be expected according to current views on the structure of curved DNA. A major difference is in the analysis of the data. We did not try to determine a degree of curvature from our experimental data; it is clear from our simulations that this would be possible only, if we would arbitrarily fix some parameters of the DNA double helices. We have used the model of Bolshoy et al. [13] as a basis of our interpretation, because this model appears to be sufficiently well justified. We find that this model is consistent with our data, when we use the special hydrodynamic properties described above. An increased rigidity of curved DNA fragments has been suggested previously by Levene et al. [5] based on a model with high internal mobility. As discussed above, we have to use a different model from that applied by Levene et al. and get the Bolshoy et al. model to agree with our experimental data only in the limit of low internal mobility of the curved DNA fragments. Obviously our conclusions are subject to the validity of the Bolshoy et al. model, but our conclusions remain valid even if DNA curvature is slightly overestimated by this model.

A contribution from slow modes of internal conversion in curved DNA segments appears to be attractive not only for the explanation of our electrooptical data but also as a factor contributing to the unusually low mobility of curved DNA fragments during gel electrophoresis. In summary, the results obtained on the curved DNA fragments analyzed in the present investigation indicate that their average degree of "deviations from linearity" is not much different from that of standard DNA fragments. However, these results are consistent with the view that curved DNA is "curved" preferentially in one direction, whereas standard DNA is "bent" by thermal motions in virtually all directions with equal probability. Our results also indicate that the dynamic persistence length of curved DNA is in the range around 1000 Å and that there is a major component of the internal dynamics with a relatively low rate.

Acknowledgements

The technical assistance of Bettina Krahmer and Jürgen Wawrzinek is gratefully acknowledged. We are indebted to Drs. Edward Trifonov and Alexander Bolshoy for a copy of their program. For our computations we used the facilities of the Gesellschaft für wissenschaftliche Datenverarbeitung mbH, Göttingen.

References

1 E.N. Trifonov, CRC Crit. Rev. Biochem. 19 (1985) 89.
2 P.J. Hagerman, Annu. Rev. Biochem. 59 (1990) 755.
3 J.C. Marini, S.D. Levene, D.M. Crothers and P.T. England, Proc. Natl. Acad. Sci. USA 79 (1982) 7664; Correction: J.C. Marini and P.T. Englund, Proc. Natl. Acad. Sci. U.S.A. 80 (1983) 7678.
4 P.J. Hagerman Proc. Natl. Acad. Sci. U.S.A. 81 (1984) 4632.
5 S.D. Levene, H.M. Wu and D.M. Crothers, Biochemistry 25 (1986) 3988.
6 S. Diekmann and D. Porschke, Biophys. Chem. 26 (1987) 207.
7 D. Porschke, N. Geisler and W. Hillen, Nucleic Acids Res. 10 (1982) 3791.
8 D. Porschke, Biopolymers 28 (1989) 1383.
9 L. Ulanovsky, M. Bodner, E.N. Trifonov and M. Choder, Proc. Natl. Acad. Sci. U.S.A. 83 (1986) 862.
10 H.S. Koo, J. Drak, J.A. Rice and D.M. Crothers, Biochemistry 29 (1990) 4227.
11 C.H. Laundon and J.D. Griffith, Biochemistry 26 (1987) 3759.
12 D. Porschke and A. Obst, Rev. Sci. Instrum. 62 (1991) 818.
13 A. Bolshoy, P. McNamara, R.E. Harrington and E.N. Trifonov, Proc. Natl. Acad. Sci. U.S.A. 88 (1991) 2312.
14 P. De Santis, A. Palleschi, M. Savino and A. Scipioni, Biophys. Chem. 32 (1988) 305.
15 J. Garcia de la Torre and V.A. Bloomfield, Q. Rev. Biophys. 14 (1981) 81.
16 J. Antosiewicz and D. Porschke, J. Phys. Chem. 93 (1989) 5301.
17 P.J. Hagerman and B.H. Zimm, Biopolymers 20 (1981) 1481.
18 D. Porschke and G. Nolte, Biopolymers 30 (1990) 1289.
19 W.A. Wegener, R.M. Dowben and V.J. Koester, J. Chem. Phys. 70 (1979) 622.
20 T. Hankeln, Dissertation, Universität Bochum (1990).
21 M. Colpan and D. Riesner, J. Chromatogr. 296 (1984) 339.

22 H.H. Grünhagen, Ph.D. Thesis, Universität Braunschweig (1974).
23 D. Porschke, Nucleic Acids Res. 8 (1980) 1591.
24 J. Antosiewicz and D. Porschke, Biophys. Chem. 33 (1989) 19.
25 D. Porschke, K. Tovar and J. Antosiewicz, Biochemistry 27 (1988) 4674.
26 D. Porschke and M. Jung, J. Biomol. Struct. Dyn. 2 (1985) 1173.
27 S.W. Provencher, Biophys. J. 16 (1976) 27.
28 S. Diekmann, W. Hillen, B. Morgeneyer, R.D. Wells and D. Porschke, Biophys. Chem. 15 (1982) 263.
29 D. Porschke, J. Biomol. Struct. Dyn. 4 (1986) 373.
30 D. Porschke, Biophys. Chem. 40 (1991) 169.
31 G.S. Manning, Quart. Rev. Biophys. 11 (1978) 179
32 M.T. Record, Quart. Rev. Biophys. 11 (1978) 103.
33 J. Antosiewicz, G. Nolte and D. Porschke, Macromolecules 25 (1992) 6500.
34 M. Le Bret, C.R. Acad. Sci. Paris 292 (1981) 291.
35 M. Fixman, J. Chem. Phys. 76 (1982) 6346.
36 D.G. Alexeev, A.A. Lipanov and I.Y. Skuratovskii, J. Biomol. Struct. Dyn. 4 (1987) 989.
37 H.S. Park, S. Arnott, R. Chandrasekaran, R.P. Millane and F. Campagnari, J. Mol. Biol. 197 (1987) 513.
38 K. Yanagi, G.G. Prive and R.E. Dickerson, J. Mol. Biol. 217 (1991) 201.
39 T.M. Birshtein and O.B. Ptitsyn, J. Polym. Sci. C16 (1969) 4617.
40 K.E. Reinert, Biophys. Chem. 13 (1981) 1.
41 E.N. Trifonov, R.K.Z. Tan and S.C. Harvey, in: DNA bending and curvature, eds. W.K. Olson, M.H. Sarma, R.H. Sarma and M. Sundaralingam (Adenine Press, New York, 1987) p. 243.
42 S.A. Allison and P. Nambi, Macromolecules 25 (1992) 759.